RASĀYAN *J. Chem.*
Vol. 19 | No. 2 | 754-765|April-June | 2026
ISSN: 0974-1496 | e-ISSN: 0976-0083 | CODEN: RJCABP
http://www.rasayanjournal.com
http://www.rasayanjournal.co.in

A STUDY ON SYNTHESIS AND LUMINESCENCE PROPERTIES OF NOVEL B_2O_3-TeO_2-Al_2O_3-MgO-Dy_2O_3 GLASSES FOR WHITE LIGHT EMITTING

P. Pavithra, Thummala Chengaiah and Borelli Devaprasad Raju✉
Department of Physics, Sri Venkateswara University, Tirupati-517502, (A.P) INDIA
✉Corresponding author: drdevaprasadraju@gmail.com

ABSTRACT

The present investigation used the conventional melt-quenching technique to create an entirely novel set of dysprosium (Dy^{3+}) ion-doped boro-tellurite–alumino–magnesium oxide (BTAMDy) spectacles that contained various percentages of Dy_2O_3. While the Fourier transform infrared (FTIR) spectra showed discrete vibrational bands associated with TeO_4 and BO_3 structural units, the X-ray diffraction (XRD) patterns verified that the produced spectacles had an amorphous composition. Additionally, to investigate the surface characteristics as well as confirm consistent constituent dispersion across the samples, scanning electron microscopy (SEM) in conjunction with energy-dispersive X-ray spectroscopy (EDS) was utilized. Based on the Judd–Ofelt (J–O) formalism, optical absorption analysis produced intensity values (Ω_2, Ω_4, Ω_6) that followed the trend $\Omega_2 > \Omega_6 > \Omega_4$, indicating a highly asymmetric and covalent environment surrounding Dy^{3+} ions. The photoluminescence spectra showed a mild red emission ($^4F_{9/2} \rightarrow {}^6H_{11/2}$) together with strong blue ($^4F_{9/2} \rightarrow {}^6H_{15/2}$) and yellow ($^4F_{9/2} \rightarrow {}^6H_{13/2}$) transitions under stimulation at 350 nm. According to lifetime measurements of the $^4F_{9/2}$ level, the highest emission intensity was recorded at 0.5 mol% Dy_2O_3, after which concentration quenching took place. The yellow-to-blue (Y/B) luminosity ratio, associated colour temperature (CT), and computed CIE spectrum dimensions were used to assess the close to white light emission behaviour. By tuning the Dy^{3+} ion concentration within the boro-tellurite-alumino-magnesium glass network, this study highlights the material's capability for applications involving white LEDs and solid-state lighting, demonstrating efficient near-white luminescence performance.

Keywords: Boro tellurite glasses, optical absorption, Photoluminescence, Dy^{3+} ions, white LEDs, Radiative transition probability.

RASĀYAN *J. Chem.*, Vol. 19, No. 2, 2026

INTRODUCTION

Due to its unique optical properties, doped with ions of rare earth elements (RE) has experienced a significant increase in recent years., which arises from intra-4f electronic transitions that remain shielded by the outer filled electron shells.[1,2] Glass hosts outperform ceramics and phosphors in terms of chemical stability, ease of manufacture, the capacity to include large RE-ion concentrations, and low-cost processing.[3-5] Because of these benefits, RE-doped glasses have emerged as important materials for numerous photonic technologies, including solid-state lasers, optical amplifiers, field-emission displays, sensors, infrared-to-visible up-conversion systems, nonlinear optical devices, and white light-emitting diodes (w-LEDs).[6-9] Dysprosium (Dy^{3+}) is a prominent RE ion due to its strong visual emissions, particularly the blue ($^4F_{9/2} \rightarrow {}^6H_{15/2}$, ~480 nm) and yellow ($^4F_{9/2} \rightarrow {}^6H_{13/2}$, ~575-590 nm) transitions.[10,11] Dy^{3+} is an effective activator for solid-state lighting and w-LED applications due to its ability to generate white light.[12] Dy^{3+} ions are known for their outstanding color purity, great emission intensity, and quantum efficiency when placed in an appropriate glass network.[13] Developing Dy^{3+}-doped glasses with specific host compositions is crucial for improving performance in visible photonic devices. Several host systems, including borate, phosphate, silicate, and tellurite glasses, have been investigated for this purpose.[14-16] Boro tellurite glasses are distinctive materials that merge the robust structural characteristics of borate systems with the superior optical performance associated with tellurite-based glasses. Due to the presence of stable structural units such as diborate, triborate, tetraborate, and pentaborate, borate compositions are valued for their excellent glass-forming ability and high thermal stability. These units support the establishment of a solid, three-dimensional community that is also interconnected. The tellurite glasses have a low phonon energy (800–900 cm^{-1}), a high refraction index and high RE-ion solubility, which reduces non-radiative relaxation and improves luminescence efficiency.[17,18] As a result,

borotellurite glasses have good optical transparency, chemical durability, and thermal stability, making them ideal materials for w-LEDs, lasers, and nonlinear optical systems.[19] By adding appropriate network modifiers, borotellurite glasses can improve their structural and optical properties even further. Al_2O_3 enhances cross-linking in glass, improving thermal and mechanical stability.[20] Similarly, MgO alters the local field around RE ions, reducing ion clustering and improving both transparency and structural stability.[21] The presence of such oxides strengthens the glass network and lowers phonon-assisted non-radiative losses, resulting in higher optical efficiency.[22] This work focuses on the preparation and detailed investigation of Dy^{3+}-doped borotellurite glass systems consisting of B_2O_3-TeO_2-Al_2O_3-MgO-Dy_2O_3. The synthesized glasses are examined using XRD to verify their amorphous nature, FTIR spectroscopy to study structural features, and SEM combined with Energy Dispersive X-ray (EDX) analysis to observe surface morphology and confirm dispersion of elements. Optical characteristics are explored through UV–visible absorption spectroscopy along with Judd–Ofelt (J–O) analysis, while photoluminescence (PL) measurements are utilized to assess emission behaviour and chromaticity. Overall, the study aims to understand the structural and luminescence performance of Dy^{3+}-activated borotellurite glasses and determine their suitability for advanced solid-state lighting, including near-white light emission applications.

EXPERIMENTAL

Fabrication of Dy^{3+} Glasses

A series of Dy^{3+}-doped borotellurite glasses with the composition (B_2O_3–TeO_2–Al_2O_3–MgO)–xDy_2O_3, where the traditional melt-quenching process was used to create x = 0.1, 0.5, 1.0, 1.5, and 2.0 mol%. High-purity (≥99.9%) B_2O_3, TeO_2, Al_2O_3, MgO and Dy_2O_3, powders were carefully weighed with ±0.0001 g precision and mixed in proportions of stoichiometry. To guarantee consistency, the powdered materials had been subsequently carefully mixed and pounded using a mortar made of agate for nearly half an hour. The resulting combination has been placed in a silica crucible and heated for nearly ninety minutes at 1100°C in an electric muffle furnace. During melting, the melt was intermittently stirred with an alumina rod to enhance chemical homogeneity and remove trapped air bubbles. The glass specimens were formed by pouring the resultant transparent melt onto a metal mould that had been preheated and pressing it right away onto a different hot plate. The previously quenching specimens were then dried for 10 hours at 400°C, a temperature close to the glass transition point, to relieve internal stress. The specimens have been gradually cooled to room temperature within the furnace following annealing. The solidified glasses were cut and polished to obtain optically smooth specimens with a thickness ranging from 1–3 mm, suitable for optical and spectroscopic characterisation. The prepared glasses were labelled BTAMDy01, BTAMDy05, BTAMDy10, BTAMDy15, and BTAMDy20 based on the Dy_2O_3 concentration levels of 0.1, 0.5, 1.0, 1.5, and 2.0 mol%, respectively, as illustrated in Fig.-1.

Fig.-1: Dy^{3+} Doped Borotellurite Glass Samples(BTAMDy Glasses)

Instrumentation and Analytical Methods

Conventional characterization methods were utilized for evaluating the BTAMDy glass specimens' optical and physical characteristics. Using distilled water to serve as the immersion medium, every specimen's concentration was estimated using Archimedes' principle. An Abbe refractometer with a sodium vapor light source (λ = 589.3 nm) and 1-bromonaphthalene as the interface liquid was utilized to calculate the refractive index of the substance. To confirm the amorphous structure, XRD analysis was carried out using a RIGAKU diffractometer within the 2θ range of 5°–90°. The structural vibrations were investigated using FTIR spectroscopy using a Bruker Alpha-II instrument at room temperature, recorded with a resolution of 4 cm^{-1} over the 500–4000 cm^{-1} spectral range. Surface microstructure and elemental

distribution were analysed using a JEOL JSM-IT500LV scanning electron microscope equipped with an EDS system. A Jasco V-570 spectrophotometer was used to acquire optical absorption spectra in the UV, visible, and near-IR ranges. An Edinburgh Instruments FLS980 spectrofluorometer was used to record photoluminescence excitation and emission spectra at a spectral resolution of 1 nm and an excitation wavelength of 350 nm. The lifetime decay of the $^4F_{9/2}$ excited state of Dy^{3+} ions was also measured using the same setup. All experiments were carried out under ambient conditions.

RESULTS AND DISCUSSION

Physical Characteristics

In BTAMDy glasses, Table-1 illustrates how the physical attributes change with the concentration of Dy^{3+} ions. Important details on the glass network's structural development and applicability to optoelectronic applications are revealed by the systematic trends that have been found. As the Dy^{3+} content rises, the glasses' density steadily increases from 4.731 to 5.042 g cm^{-3}, while their molar volume stays relatively constant (17.661–17.744 cm^3 mol^{-1}). This shows that Dy^{3+} ions were successfully incorporated into the borotellurite matrix without significantly altering its structure, improving the glass network's compactness. A rise in molar refraction (R_m) (6.447–6.535 cm^3) and molar electronic polarizability (α_m) (2.556–2.591 $\times$ 10^{-24} cm^3) coincides with a similar increase in refractive index (n) from 1.652 to 1.658. These changes are a result of Dy–O bonding-induced improved electronic polarizability, which raises the optical density of the glass. These enhancements help to improve light extraction and confinement efficiency, which is beneficial for w-LED applications. With Dy^{3+} doping, the optical dielectric constant (ε_{opt}) slightly increases (2.729–2.749), whereas the metallization factor (M) somewhat reduces (0.634 → 0.631). The glasses maintain their non-metallic nature and superior insulating properties since M values stay below unity for all compositions.[23] By reducing non-radiative losses, this decrease of free carrier density promotes effective luminescence. High optical transparency and low interfacial reflection—qualities that are preferred for glass hosts in solid-state lighting—are confirmed by the reflectance (R%), which shows a slight increase from 6.04 percent to 6.13 percent. As the Dy^{3+} concentration increases, the ions progressively move closer together, which is indicated by the noticeable reduction in inter-ionic spacing (r_i) from 24.202 Å to 9.290 Å, along with a substantial rise in ionic concentration (C) from 0.056 to 1.127 mol L^{-1}. The number density of Dy^{3+} ions (N) consequently rises from 0.340 $\times$ 10^{20} to 6.787 $\times$ 10^{20} ions cm^{-3}, indicating a closer separation between Dy^{3+} and Dy^{3+}. Excessive clustering can cause concentration quenching through cross-relaxation mechanisms, whereas moderate doping increases emission intensity. Finding the ideal Dy^{3+} concentration is therefore essential to balancing luminescence efficiency and reducing quenching effects. The structural compactness and electronic polarizability of borotellurite glasses are dramatically influenced by Dy^{3+} ions, as evidenced by the systematic evolution of density, refractive index, molar refraction, dielectric constant, and ionic concentration with Dy^{3+} incorporation. These compositional modifications further confirm the suitability of Dy^{3+}-doped borotellurite glasses as promising host materials for w-LED technology and other advanced photonic devices.[24]

Table-1: Physical Characteristics of BTAM-doped Dy^{3+} Glasses

S. No.	Physical Properties	BTAMDy0.1	BTAMDy0.5	BTAMDy1.0	BTAMDy1.5	BTAMDy2.0
1	Thickness (cm)	0.343	0.348	0.335	0.359	0.342
2	Refractive index (n)	1.652	1.653	1.655	1.656	1.658
3	Density (g/cm^3)	4.731	4.810	4.892	4.964	5.042
4	Molar volume V_m (cm^3/mol))	17.661	17.630	17.652	17.710	17.744
5	Molar Refraction R_m (cm^3)	6.447	6.457	6.478	6.514	6.535
6	Ionic Concentration (mol/L)	0.056	0.283	0.566	0.846	1.127
7	Inter ionic distance r_i (A^0)	24.202	15.272	12.103	10.443	9.290
8	Molar electronic polarizability, α_m (10^-	2.556	2.560	2.568	2.582	2.591

	^{24} cm^3)					
9	Optical dielectric constant (ϵ_{opt})	2.729	2.732	2.739	2.742	2.749
11	Metallization factor M	0.634	0.633	0.633	0.632	0.631
12	Reflection loss R (%)	6.04	6.06	6.09	6.10	6.13
13	Concentration N (ions / cm^3) (x10^{20})	0.340	1.707	3.411	5.100	6.787

X-ray Diffraction (XRD) Analysis

Figure-2 displays the XRD patterns of the BTAMDy glass specimens. All samples exhibit a broad, diffused hump without any sharp Bragg reflections, confirming their non-crystalline (amorphous) structure. The diffraction measurements were recorded at room temperature using a RIGAKU XRD instrument over the 2θ scan range of 5° to 90°. The appearance of a large hump in the lower scattering region is characteristic of non-crystalline materials and is due to the long-range structural chaos and short-range atomic groupings found in amorphous glasses.[25] The absence of prominent Bragg reflections suggests that no crystalline phases occur during the glass formation process, even after Dy_2O_3 inclusion. These observations demonstrate that Dy^{3+} ions successfully incorporate into the borotellurite network without causing devitrification or phase separation. As a result, the acquired XRD patterns significantly support the amorphous nature and structural homogeneity of the produced BTAMDy glass system.

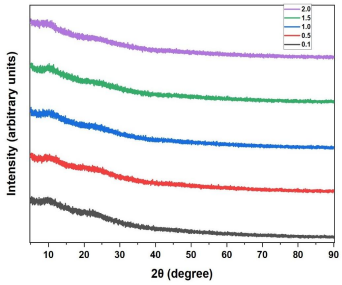

Fig.-2: XRD Spectra of Dy^{3+} Doped Borotellurite Glasses

FTIR Spectral Study

Figure-3 shows the FTIR spectra of Dy^{3+}-doped borotellurite glasses at different Dy_2O_3 concentrations. The spectra contain multiple distinct absorption bands that correspond to the basic vibrations of borate and tellurite structural components. Te-O stretching vibrations linked to TeO_3 and TeO_3 structural groups are responsible for the wide band around 695 cm^{-1}. The shoulder at 838 cm^{-1} is caused by Te-O bending vibrations in trigonal TeO_3 units, indicating tellurite links in the network.[26] The absorption peak observed around 1083 cm^{-1} is ascribed to the symmetric stretching vibration of BO_4 tetrahedral groups[27], while the feature near 1257 cm^{-1} is associated with B–O stretching within BO_3 units linked to boroxol ring structures. Additionally, the band appearing close to 1357 cm^{-1} corresponds to the stretching modes of trigonal BO_3 groups, confirming the glass network has both BO_3 and BO_4 structural elements.[28] These absorption bands' concurrent development reveals a mixed borotellurite glass network comprising both BO_3/BO_4 and TeO_3/TeO_6 structural units. Dy^{3+} ions operate as a network modifier, altering the local bonding environment while maintaining the glass's amorphous structure. Structural modifications improve compactness and stability, resulting in better optical and luminous performance in Dy^{3+}-doped glass systems.

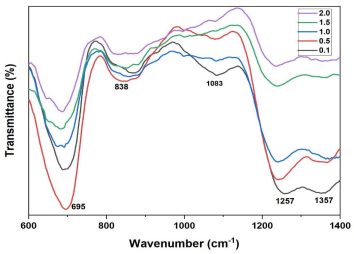

Fig.-3: FTIR Spectra of Dy^{3+} Doped Borotellurite Glasses

SEM and EDX Analysis

The surface features of the 1.0 mol% Dy^{3+}-doped borotellurite glass were studied using SEM, as shown in Fig.-4a. A fracture morphology characteristic of amorphous glass is indicated by the micrograph's comparatively rough surface and unevenly formed particles. The produced glass's non-crystalline character is confirmed by the lack of distinct crystalline phases or grain boundaries. According to the microstructural characteristics, Dy^{3+} ions are evenly dispersed throughout the glass network without causing phase separation or micro-crystallisation. The EDX spectrum of the 0.1 mol % Dy^{3+}- doped glass (Fig.-4b) shows distinct elemental peaks corresponding to Te, B, Al, Mg, O, and Dy, confirming the nominal chemical composition. The obvious presence of the Dy peak demonstrates that dysprosium ions were successfully incorporated into the borotellurite glass matrix.[29] Furthermore, the absence of extraneous peaks indicates that the synthesized materials are impurity-free, ensuring compositional homogeneity and chemical purity.

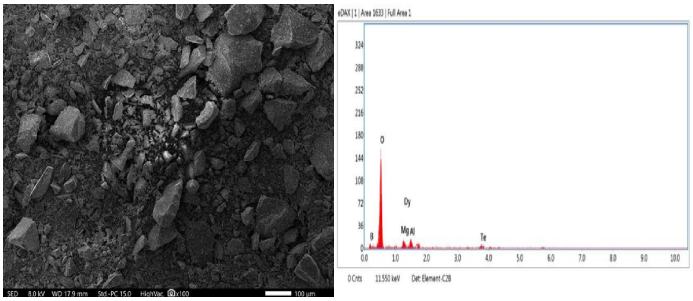

(a) (b)

Fig.-4: SEM Image with EDX Spectra of Dy^{3+} Doped Borotellurite Glasses

Spectral Absorption Features and Judd–Ofelt Modelling

The Dy^{3+}-doped borotellurite glass samples' optical absorption spectra were studied in the 300–1800 nm wavelength range to investigate the distinctive electronic transitions that originate from the $^6H_{15/2}$ ground state of Dy^{3+} ions. The recorded spectra, shown in Fig.-5(a) (VIS) and 5(b) (NIR), show well-defined absorption bands corresponding to the intra-4f transitions characteristic of trivalent dysprosium. Absorption peaks at 346, 382, 426, 448, and 473 nm are caused by the $^6H_{15/2} \rightarrow {}^{6P}{}_{5/2}$, $^4I_{13/2}$, $^4G_{11/2}$, $^4I_{15/2}$, and $^4F_{9/2}$ transitions, respectively. The near-infrared region has transitions at 752, 806, 898, 1088, 1264, and 1657 nm. These correspond to the $^6H_{15/2} \rightarrow {}^6F_{3/2}$, $^6F_{5/2}$, $^6F_{7/2}$, $^6H_{7/2}$, $^6F_{11/2}$, and $^6H_{11/2}$ levels. Among these, the band at 1264 nm ($^6H_{15/2} \rightarrow {}^6F_{11/2}$) exhibits the highest intensity, indicating a hypersensitive transition associated with the asymmetric and Covalent character of Dy–O coordination in the matrix of glass. The sharp and well-defined absorption peaks, without noticeable splitting, confirm a homogeneous distribution of Dy^{3+} ions within the amorphous network.[30] The experimental oscillator strengths (f_{exp}) for the detected transitions were computed using the integrated absorption cross-section, while the theoretical values (f_{cal}) were obtained using the Judd–Ofelt (J–O) theoretical model. A comparison of these values, presented in Table-2, reveals good agreement between experimental and theoretical results, with only minor deviations attributed to weak transition probabilities and the neglect of higher-order relativistic effects. The root mean square (RMS) deviation ($\delta_{rms} = \pm 0.54 \times 10{-}6$) lies within acceptable limits, confirming the reliability of the fitting procedure. The Judd-Ofelt parameters are displayed in Table-3. (Ω_2, Ω_4, and Ω_6) serve as key indicators of the symmetry and chemical environment experienced by Dy^{3+} ions within the glass network.

The relatively higher Ω_2 value indicates a strong covalent character and significant asymmetry in the Dy–O coordination, accounting for the hypersensitive transition seen in the NIR spectrum. The trend $\Omega_2 > \Omega_6 > \Omega_4$ suggests that short-range interactions dominate over long-range field effects in the glass matrix.[31] Overall, the high oscillator strengths and pronounced hypersensitive transitions confirm that Dy^{3+}ions occupy low-symmetry, covalently bonded sites within the borotellurite framework. The results show that these materials are potential candidates for use in photonic and white light applications because of their advantageous optical properties and the efficiency of their f-f transitions.

Table-2: The calculated oscillator strengths (f_{cal} x 10^{-6}) and experimental oscillator strengths (f_{exp} x 10^{-6}) of Dy^{3+}-doped BTAM glasses were compared with those reported for other Dy^{3+}-doped glasses in the literature

S.No.	Transitions	Wavenumber (cm^{-1})	BTAMDy 1.0		PKANbDy1.0 [32]		TSWD1.0 [33]	
			f_{exp}	f_{cal}	f_{exp}	f_{cal}	f_{exp}	f_{cal}
1	$^6P_{5/2}$	28521	0.916	0.017	0.42	1.04	-	-
2	$^4I_{13/2}$	24796	1.749	1.056	1.16	1.56	-	-
3	$^4G_{11/2}$	23624	0.592	0.127	0.32	0.05	-	-
4	$^4I_{15/2}$	21423	0.623	0.643	0.54	0.92	0.02	1.04
5	$^4F_{9/2}$	20176	0.098	0.217	-	-	0.05	0.36
6	$^6F_{3/2}$	14621	0.841	0.236	-	-	0.39	0.41
7	$^6F_{5/2}$	13932	2.356	1.359	1.56	1.58	2.84	2.19
8	$^6F_{7/2}$	12795	3.695	3.216	4.39	3.02	4.88	4.63
9	$^6H_{7/2}$	9317	4.019	4.269	-	-	5.40	5.43
10	$^6F_{11/2}$	6958	10.196	10.072	18.76	18.68	17.22	17.21
11	$^6H_{11/2}$	426	0.137	0.398	2.27	2.80	2.99	3.05

Table-3: The Judd-Ofelt Ω_λ (λ = 2, 4, 6) (10^{-20} cm^2) parameters of BTAM Doped with Dy^{3+}, as well as the corresponding values for other types of glasses

S.No.	Glass	Ω_2	Ω_4	Ω_6	Trend	Reference
1	BTAMDy1.0	11.46	4.13	9.32	$\Omega_2>\Omega_6>\Omega_4$	Present work
2	YCaSBDy0.5	2.84	0.15	0.95	$\Omega_2>\Omega_6>\Omega_4$	[34]
3	DyZB10P	3.95	0.91	1.95	$\Omega_2>\Omega_6>\Omega_4$	[35]
4	BZBdy	4.03	1.14	1.65	$\Omega_2>\Omega_6>\Omega_4$	[36]

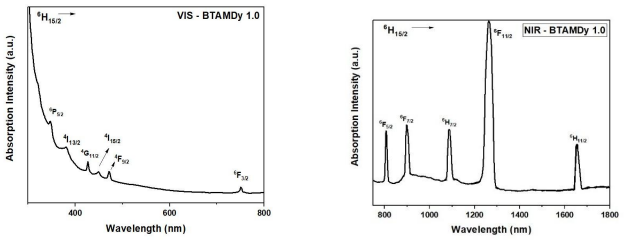

(a) (b)

Fig.-5: Optical Absorption Spectra of Dy^{3+} Doped Borotellurite Glasses

Excitation Study

Figure-6 shows the excitation spectra of borotellurite glasses doped with Dy^{3+}, ranging from 300 to 700 nm, with an emission measured at 575 nm. The spectra show four excitation bands at 323, 350, 364, and 386 nm. These bands are the outcome of Dy^{3+} ion transitions. $^6H_{15/2} \rightarrow {}^4M_{17/2}$, $^6H_{15/2} \rightarrow {}^6P_{7/2}$, $^6H_{15/2} \rightarrow {}^6P_{5/2}$, and $^6H_{15/2} \rightarrow {}^4I_{13/2}$. The $^6H_{15/2} \rightarrow {}^6P_{7/2}$ transition at 350 nm has the highest intensity and dominates the excitation process. This length was chosen to extract the Dy^{3+} ions, and the emission spectra corresponding to each video sample were then recorded. The excitation intensity gradually increased with the increase in Dy^{3+} concentration upto 1.0 mol%, after which it gradually decreased.[37] This pattern implies that at higher dopant levels, concentration quenching occurs as a result of non - radiative energy transfer between closely spaced Dy^{3+} ions. The glass network's structural disorder and the fluctuating local ligand environments surrounding Dy^{3+} ions are reflected in the broadening of excitation bands. The distinct and abrupt peaks support the intra-configurational 4f–4f character of Dy^{3+} transitions, which are only marginally impacted by the matrix environment. A pure electronic transition is observed in the corresponding excitation band at 350 nm, which also provides information about the local symmetry around the Dy^{3+} ions in the glass matrix.[38] The acquired spectral pattern confirms that Dy^{3+} ions were successfully incorporated into the borotellurite network without altering its amorphous nature, since it is compatible with previously reported Dy^{3+} doped oxide and tellurite glasses.

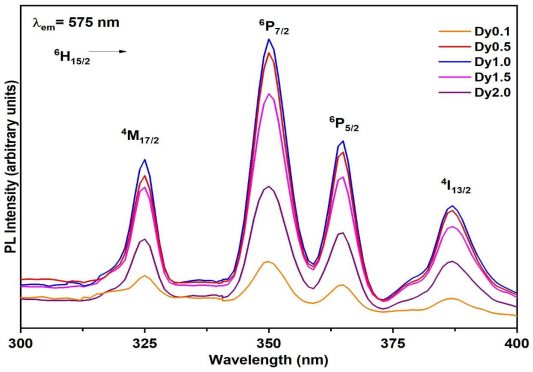

Fig.-6: Excitation Spectra Monitored at 575 nm Emission

Emission Study

Figure-7 presents the photoluminescence spectra of Dy^{3+}-doped borotellurite glass samples under 350 nm excitation. The spectra reveal three distinct emission peaks located near 483, 575, and 665 nm, which are assigned to the $^4F_{9/2} \rightarrow {}^6H_{15/2}$, $^4F_{9/2} \rightarrow {}^6H_{13/2}$, and $^4F_{9/2} \rightarrow {}^6H_{11/2}$ electronic transitions of Dy^{3+} ions, respectively. The blue emission, which appears at 483 nm, is the result of a magnetic dipole transition; the yellow emission, which occurs at 575 nm, is the result of an electrical dipole transition that is highly sensitive to the asymmetry of the local field around the Dy^{3+} ions.[39] The dominance of the yellow band over the blue one indicates that Dy^{3+} ions occupy sites without inversion symmetry in the borotellurite glass matrix. As the Dy^{3+} concentration increases, the emission intensity steadily rises and reaches its maximum at 1.0 mol%, after which it drops due to concentration quenching. This reduction in intensity at higher dopant levels is likely caused by non-radiative energy transfer processes, including cross-relaxation and multiphonon interactions between closely spaced Dy^{3+} ions. Therefore, 1.0 mol% is identified as the optimum dopant level for achieving maximum luminescence efficiency in this glass system.[40] The results of the Judd-Ofelt[41] analysis are shown in Table-4 for various radiative properties, such as radiative transition probability (A_R), stimulated emission cross-section (σ_{se}), the radiative lifetime (τ_R), the gain bandwidth ($\sigma_{se} \times \Delta\lambda_p$), and the optical gain ($\sigma_{se} \times \tau_R$). The results clearly shows the corresponding electronic transition, $^4F_{9/2} \rightarrow {}^6H_{13/2}$ at 575 nm, exhibits larger σ_{se} and gain bandwidth values than the blue emission transition, $^4F_{9/2} \rightarrow {}^6F_{15/2}$ at 483 nm. Among all compositions, the BTAMDy1.0 glass exhibits the highest A_R (2.74 $s^{-1} \times 10^3$), σ_{se} (11.5 $\times 10^{-21}$ cm^2), gain bandwidth (3.87 $\times 10^{-27}$ cm^3), and optical gain (10.6 $\times 10^{-24}$ cm^2s), confirming its superior radiative efficiency and enhanced stimulated emission probability. At higher Dy^{3+} concentrations ($\geq$ 1.5 mol %), the decrease in these parameters results from energy migration and non-radiative loss channels among adjacent Dy^{3+} ions.[42] Consequently, 1.0 mol % Dy^{3+} is established as the optimum concentration for achieving maximum optical gain and emission efficiency. The excellent gain characteristics and dominant yellow emission suggest that Dy^{3+}activated borotellurite glasses are promising materials for visible laser and photonic amplifier applications, particularly in the yellow spectral region.

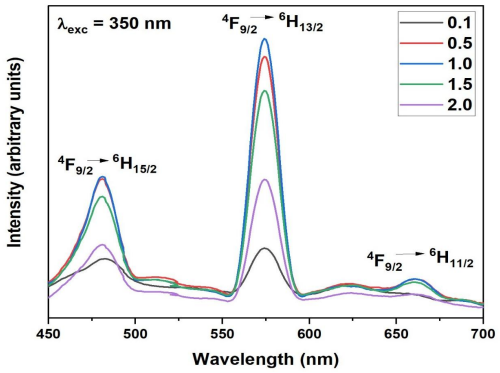

Fig.-7: Emission Spectra Under 350 nm Excitation

Table-4: The radiative transition probability (A_R) (S^{-1}), stimulated emission cross-section (σ_{se}) ($\times 10^{-21}$), radiative lifetime τ_R (μs), gain bandwidth (σ_{se} x $\Delta\lambda_p$) ($\times 10^{-27}$), and optical gain (σ_{se} x τ_R) ($\times 10^{-24}$) for the most significant emission transitions are observed in the Dy^{3+}-doped BTAM glasses.

Glass	$A_R(s^{-1})$	σ_{se} ($\times 10^{-21}$)	τ_R(μs)	Gain bandwidth ($\times 10^{-27}$)	Optical gain ($\times 10^{-24}$)
$^4F_{9/2} \rightarrow {}^6H_{15/2}$ λ = 483 nm					
BTAMDy0.1	2.30	7.6	1260	3.15	9.5
BTAMDy0.5	2.65	10.4	980	3.52	9.9
BTAMDy1.0	2.74	11.5	910	3.87	10.6
BTAMDy1.5	2.55	6.6	880	3.13	8.4
BTAMDy2.0	1.35	5.2	1000	2.87	7.0
$^4F_{9/2} \rightarrow {}^6H_{13/2}$ λ = 575 nm					
BTAMDy0.1	3.00	19.7	1250	6.87	21.2
BTAMDy0.5	5.37	37.4	990	12.16	35.8
BTAMDy1.0	6.19	42.7	565	14.10	27.8
BTAMDy1.5	5.64	29.7	651	13.15	19.4
BTAMDy2.0	4.62	19.2	800	11.40	16.8

Lifetime Analysis

Figure-8 shows the emission decay profile corresponding to the excited level ($^4F_{9/2}$) of Dy^{3+} ions in the borotellurite glass system under 350 nm excitation and 575 nm emission . The decay curve clearly deviates from a single-exponential behavior and is well fitted with a bi-exponential function, indicating the presence of multiple local environments around Dy^{3+} ions in the glass matrix. This non-exponential nature suggests that Dy^{3+} ions occupy different sites with varying ligand fields, resulting in heterogeneous relaxation dynamics. Such behavior is typical of highly polarizable glass systems and is mainly attributed to energy migration and cross-relaxation processes between neighboring Dy^{3+} ions.[43] The fitted decay parameters confirm the contribution of both fast and slow components, representing different relaxation pathways. The average lifetime (τ_{avg}) for the 1.0 mol% Dy^{3+}-doped sample is found to be approximately ~337 μs, indicating efficient radiative relaxation with moderate non-radiative losses. At this concentration, a favorable balance between luminescence intensity and lifetime is achieved, suggesting efficient energy utilization before the onset of significant concentration quenching. At higher concentrations, the reduction in lifetime is generally associated with increased non-radiative energy transfer among Dy^{3+} ions due to decreased interionic distance. Cross-relaxation and multiphonon interactions become more prominent, leading to faster decay.[44] Therefore, 1.0 mol% Dy^{3+} is identified as the optimal concentration for achieving stable and efficient luminescence, making it suitable for white light emission in the present borotellurite glass system.

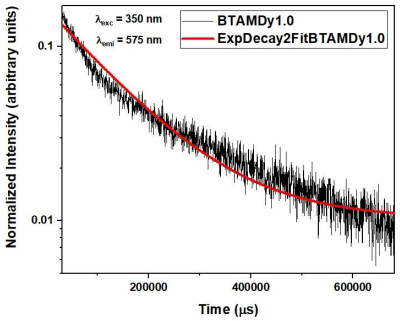

Fig.-8: Lifetime Decay Profile of Dy^{3+} Doped Borotellurite Glasses

CCT Values and Colourimetric Analysis

In order to determine the characteristics of the colour emitted by the synthetic videos, the chromaticity coordinates of the borotellurite samples doped with Dy^{3+} were analysed using the CIE 1931 chromaticity

diagram as a reference. The corresponding colour values (x, y) were obtained from the emission spectra recorded with an excitation at 350 nm excitation, and the calculated parameters are summarized in Table-5. As seen in the CIE diagram (Fig.-9), the resulting coordinates were found to lay close to (0.36, 0.40) for all Dy^{3+} concentrations. All of the glass samples emit within the near-white to warm-white range of the visible spectrum, as indicated by the grouping of points in the same area.[45] From the calculated chromaticity coordinates, the temperature of colour correlated (CCT) values were found to vary between 4517 and 5503 K, indicating that the produced light lies in the commercially recognized white light region. These values indicate the possible suitability of the produced glasses for devices that emit white light because they lie within the color temperature range associated with daylight and fluorescent lighting. Colour saturation of the radiated colour was moderate, as indicated by the colour purity (CP) values, which ranged from 22.57% to 40.13%. Additionally, it was noted that the intensity relationship between yellow and blue (Y/B) varied slightly with Dy^{3+} concentration. Variation from 1.52 to 0.1 mol% to 2.11 to 1.0 mol%, followed by a slight decline to 2.01 to 2.0 mol%.[46] The observed change in chromacity coordinates with Dy^{3+} concentration reflects the variation in the balance between blue and yellow emission components.[47] With a CCT value of 4541 K and the most balanced Y/B ratio of any composition, the 1.0 mol% Dy^{3+} sample shows the best color rendering performance prior to the commencement of concentration quenching.[48] These glasses may be suitable options for cool white light phosphor materials in optoelectronic and photonic applications since the chromaticity points are consistently positioned within the same color zone, confirming that the emission color is stable with regard to Dy^{3+} concentration.

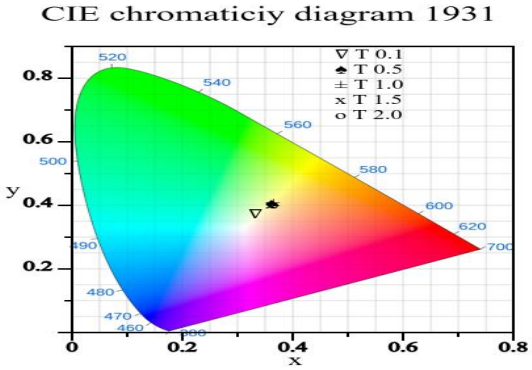

Fig.-9: CIE 1931 Chromacity Diagram of Dy^{3+} Doped Borotellurite Glasses

Table-5: CCT (correlated colour temperature), CP (colour purity), CIE (x,y) Colour Coordination, and Intensity Relationships Between Blue and Yellow (Y/B)

S. No.	Glass Samples	λ_{exc} (nm)	Color coordinates		CCT (K)	CP	Y/B ratio
			x	y			
1	BTAMDy0.1	350	0.332	0.372	5503.42	22.57	1.52
2	BTAMDy0.5	350	0.362	0.405	4642.09	38.71	2.01
3	BTAMDy1.0	350	0.366	0.407	4541.36	40.13	2.11
4	BTAMDy1.5	350	0.362	0.403	4630.18	38.06	2.09
5	BTAMDy2.0	350	0.366	0.403	4517.38	38.86	2.01

CONCLUSION

A novel set of borotellurite glasses doped with Dy^{3+} was synthesised using the traditional technique of rapid enframement. Their optical, photoluminescent, and structural characteristics were thoroughly examined. While the FTIR spectra showed the coexistence of both borate and tellurite structural units (BO_3/BO_4 and TeO_3/TeO_4), the XRD patterns verified the amorphous nature of the produced glasses. The fracture surface appeared rough and relatively homogeneous in SEM micrographs, and the EDX spectra confirmed that Dy^{3+} ions were successfully incorporated without the presence of unnecessary impurities. The trivalent state of Dy^{3+} ions within the glass network was confirmed by the optical absorption spectra, which showed distinct f – f transitions. A Judd-Ofelt analysis was used to determine the reliable intensity parameters (Ω_2, Ω_4, and Ω_6). The pattern $\Omega_2 > \Omega_6 > \Omega_4$ suggested a strong covalent bonding environment

and notable local asymmetry around Dy^{3+} ions. The emission spectra were dominated by the $^4F_{9/2} \rightarrow {}^6H_{13/2}$ transition at 575 nm, which produced bright yellow luminescence. The blue emission was caused by the $^4F_{9/2} \rightarrow {}^6H_{15/2}$ transition at 483 nm. The emission intensity increased with Dy^{3+} concentration and reached its maximum at 1.0 mol%. Beyond this level, further doping led to a reduction in luminescence due to concentration quenching, which is attributed to non-radiative energy transfer processes occurring between closely spaced Dy^{3+} ions. This behaviour was corroborated by the matching lifetime studies, which demonstrated a progressive decay time decrease with increasing dopant concentration. Following the CIE's chromaticity evaluation, all of the samples showed emission coordinates close to the white zone. The glass containing 1.0 mol% dysprosium exhibits an equilibrium yellow-to-blue (Y/B) emission intensity ratio and an appropriate correlated color correction temperature (CCT), indicating its potential for efficient white light generation. All things considered, the current work identifies Dy^{3+}-doped borotellurite glasses as viable options for optoelectronic and photonic uses, particularly in devices that output warm white light and visible lasers. The glass system's appropriateness for next-generation luminous materials is highlighted by its steady colorimetric features, efficient radiative parameters, and high asymmetry ratio.

ACKNOWLEDGMENTS

The authors are grateful to RUSA, Phase-II, Government of India, for the financial support provided through the Research Project No. UGC-III (7) RP/RUSA/ 2025, dated 29.07.2025.

CONFLICT OF INTERESTS

The authors declare that there is no conflict of interest.

AUTHOR CONTRIBUTIONS

The present work is related to *SDG-7: Affordable and Clean Energy*. All the authors contributed significantly to this manuscript, participated in reviewing/editing and approved the final draft for publication. The research profile of the authors can be verified from their ORCID ids, given below:

P.Pavithra https://orcid.org/0009-0006-6789-7897
T. Chengaiah https://orcid.org/0009-0006-2108-9317
B. Devaprasad Raju https://orcid.org/0000-0002-3485-1060

Cite this article as: P. Pavithra *et al.*, *Rasayan J. Chem.*, 19(2), 754-765(2026), https://doi.org/10.31788/RJC.2026.1929618.

REFERENCES

1. B. R. Judd, *Physical Review*, **127**, 750(1962), https://doi.org/10.1103/PhysRev.127.750
2. G. S. Ofelt, *The Journal of Chemical Physics*, **37**, 511(1962), https://doi.org/10.1063/1.1701366
3. S. O. Adeleye, A. A. Adeleke, P. Nzerem, A. I. Olosho, E. N. Anosike-Francis, T. S. Ogedengbe, J.A. Okolie, *Trends in Sciences*, **21(12)**, 8759(2024), https://doi.org/10.48048/tis.2024.8759
4. V. Kumar, S. Kumari, S. Malik, T. Ravita Sharma, A. Prasad, and A. S. Rao, *Journal of Fluorescence*, **35**, 7385(2025), https://doi.org/10.1007/s10895-024-04068-y
5. C. Julien, M. Massot, W. Balkanski, A. Krol, and W. Nazarewicz, *Materials Science and Engineering: B*, **3**, 307(1989), https://doi.org/10.1016/0921-5107(89)90026-3
6. V. P. Tuyen, B. Sengthong, V. X. Quang, P. Van Do, H. Van Tuyen, L. X. Hung and B. T. Huy, *Journal of Luminescence*, **178**, 27(2016), https://doi.org/10.1016/j.jlumin.2016.05.027
7. V. Chandrappa, Ch. Basavapoornima, V. Venkatramu, D. Shobha Rani, J. Kaewkhao, W. Pecharapa,C.K.Jayasankar,*Optik*,**266,** 169583(2022), https://doi.org/10.1016/j.ijleo.2022.169583
8. Jose A. Jimenez, Vinod Hegde, C.S. Dwaraka Viswanath, A. Richard, ACS Physical Chemitry Au, **4**, 720 (2024), https://doi.org/10.1021/acsphyschemau.4c00066
9. A. Górny, M. Kuwik, W. A. Pisarski, and J. Pisarska, *Materials*, **13**, 5022(2020), https://doi.org/10.3390/ma13215022

10. N. Mahingsa, W. Rachniyom, K. Kirdsiri, and N. Srisittiposakun, *Suan Sunandha Science and Technology Journal*,**12,** 32 (2025), https://doi.org/10.53848/ssstj.v12i1.1034
11. S. Khondara, P. Yasaka, K. Boonin, N. Intachai, S. Kothan, H. J. Kim, and J. Kaewkhao, *Radiation Physics and Chemistry*, **237**, 113007(2025), https://doi.org/10.1016/j.radphyschem.2025.113007
12. Y. Zhang, and Z. Zhu, *Journal of Non-Crystalline Solids*, **627**, 122826(2024), https://doi.org/10.1016/j.jnoncrysol.2024.122826
13. V.P. Tuyen, B. Sengthong , V.X. Quang , P. Van Do , H. Van Tuyen ,L.X. Hung, N.T. Thanh, M. Nogami, T. Hayakawa, B.T. Huy, *Journal of Non-Crystalline Solids,* **178**, 27(2016). https://doi.org/10.1016/j.jlumin.2016.05.027
14. T. Komatsu, and V. Dimitrov, *International Journal of Applied Glass Science*, 11, 253 (2019), https://doi.org/10.1111/ijag.14776
15. V. A. G. Rivera, I. C. Pinto, R. Falci, V. Fuertes, and Y. Messaddeq, *Journal of Alloys and Compounds*, **976**, 173182(2024), https://doi.org/10.1016/j.jallcom.2023.173182
16. A. M. Abdelghany, and H. A. ElBatal, *Materials and Design*, **89**, 568(2016), https://doi.org/10.1016/j.matdes.2015.09.159
17. M. I. Sayyed, A. H. Almuqrin, T. A. Hanafy, and M. Elsafi, *Optical and Quantum Electronics*, **56**, 1671(2024), https://doi.org/10.1007/s11082-024-07597-9
18. M. K. Halimah, M. A. Hazlin, and F. D. Muhammad, *Spectrochimica Acta Part A: Molecular and Biomolecular Spectroscopy*, **195**, 128(2018), https://doi.org/10.1016/j.saa.2017.12.054
19. R. G. Capelo, R. Santos Baltieri, M. de Oliveira Jr, and D. Manzani, *ACS omega*, 8, 35266 (2023), https://doi.org/10.1021/acsomega.3c05010
20. M. A. Morsy, T. F. Garrison, M. R. Kessler, M. H. Mhareb, and H. Z. El-Deen, *ACS Physical Chemistry Au*, **5**, 227(2025), https://doi.org/10.1021/acsphyschemau.4c00106
21. V. Sivaranjani, P. Deepa, P. Murugesan, A. A. Suresh, and M. Dhavamurthy, *Emergent Materials*, **8**, 1(2025), https://doi.org/10.1007/s42247-025-01079-8
22. M. P. Hehlen, M. G. Brik, and K. W. Krämer, *Journal of Luminescence*, 136, 221(2013), https://doi.org/10.1016/j.jlumin.2012.10.035
23. G. Chandrashekaraiah, N. S. Reddy, B. Sujatha, R. Viswanatha and C. N. Reddy, *Journal of Non-Crystalline Solids*, **498**, 252(2018), https://doi.org/10.1016/j.jnoncrysol.2018.06.034
24. R. Vijayakumar, R. Nagaraj, P. Suthanthirakumar, P. Karthikeyan, and K. Marimuthu, *Spectrochimica Acta Part A: Molecular and Biomolecular Spectroscopy*, **204**, 537(2018), https://doi.org/10.1016/j.saa.2018.06.092
25. I Kashif, and A. Ratep, *Results in Optics*, **11**, 100401(2023), https://doi.org/10.1016/j.rio.2023.100401
26. K. Maheshvaran, and K. Marimuthu, *In AIP Conference Proceedings,* **1349**, 581(2011), https://doi.org/10.1063/1.3605992
27. N. Yaduvanshi, C. Basavapoornima, A. S. Alqarni, U. K. Kagola, T. Uthayakumar, A. Madhu and N. Srinatha, *Optical Materials*, **151**, 115359(2024), https://doi.org/10.1016/j.optmat.2024.115359
28. S. Rada, M. Culea, and E. Culea, *Journal of Non-Crystalline Solids*, **354**, 5491(2008), https://doi.org/10.1016/j.jnoncrysol.2008.09.009
29. I. Saber, K. Dahmani, M. Galai, A. E. Magri, R. Hsissou, H. Barbita, and M. S. Elyoubi, *Optical Materials*, **149**, 115079, (2024), https://doi.org/10.1016/j.optmat.2024.115079
30. N. S. Azizan, and M. M. Yusr, *International Journal of Entrepreneurship and Management Practices*, **2**, 93(2019), https://doi.org/10.35631/ijemp.270010
31. P. Sailaja, S. Mahamuda, R. A. Talewar, K. Swapna, and A. S. Rao, *Journal of Alloys and Compounds*, **789**, 744(2019), https://doi.org/10.1016/j.jallcom.2019.03.148
32. T. Srihari, C.K. Jayasankar, *Optical Materials,* **69**, 87(2017), https://doi.org/10.1016/j.optmat.2017.04.001
33. V. Himamaheswara Rao, P. Syam Prasad, M. Mohan Babu, P. Venkateswara Rao, T. Satyanarayana, Luís F. Santos, N. Veeraiah, *Spectrochimica Acta Part A: Molecular and Biomolecular Spectroscopy,* **188**, 516(2018), https://doi.org/10.1016/j.saa.2017.07.013

34. C.R. Kesavulu, H.J. Kim, S.W. Lee, J. Kaewkhao, N. Chanthima, Y. Tariwong, *Journal of Alloys and Compounds,* **726**, 1062(2017), https://doi.org/10.1016/j.jallcom.2017.08.091
35. R. Vijaya Kumar, G. Venkataiah, K. Marimurthu, *Physica B: Condensed matter,* **457,** 287(2015), https://doi.org/10.1016/j.physb.2014.10.003
36. B. Shanmugavelu, V.V. Ravi Kanth Kumar, *Journal of Luminescence,* **146**, 358(2014), https://doi.org/10.1016/j.jlumin.2013.10.018
37. N. Wada and K. Kojima, *Journal of luminescence*, **126**, 53(2007), https://doi.org/10.1016/j.jlumin.2006.05.002
38. Y. A. Lakshmi, K. Swapna, K. R. K. Reddy, S. Mahamuda, M. Venkateswarulu,, and A. S. Rao, Optical Materials, **109**, 110328 (2020), https://doi.org/10.1016/j.optmat.2020.110328
39. P. J. Lakshmi, and K. V. Selvi, *International Journal for Modern Trends in Science and Technology*, **6**, 15(2020)
40. K. Damak, C. Rüssel, and R. Maâlej, *Journal of Quantitative Spectroscopy and Radiative Transfer*, **134**, 55(2014), https://doi.org/10.1016/j.jqsrt.2013.10.013
41. Q. Su, Z. Pei, L. Chi, H. Zhang, Z. Zhang, and F. Zou, *Journal of alloys and compounds*, **192**, 25 (1993), https://doi.org/10.1016/0925-8388(93)90174-L
42. W. Thanyaphirak, P. Yasaka, K. Boonin, , N. Sangwaranatee and J. Kaewkhao, *Suranaree Journal of Science and Technology*, **31**, 030199(2024), https://doi.org/10.55003/cast.2025.263873
43. T. Srihari, C.K. Jayasankar, *Optical Materials,* **69**, 87(2017), https://doi.org/10.1016/j.optmat.2017.04.001
44. S. Karki, , C. R. Kesavulu H. J. Kim, J. Kaewkhao, N. Chanthima, S. Kothan, and S. Kaewjaeng, *Journal of Non-Crystalline Solids*, **521**, 119483(2019), https://doi.org/10.1016/j.jnoncrysol.2019.119483
45. M. Gökçe, and D. Koçyiğit, *Optical Materials*, **89**, 568(2019), https://doi.org/10.1016/j.optmat.2019.02.004
46. N. Deopa, S. Saini, S. Kaur, A. Prasad, and A. S. Rao, *Journal of Rare earths*, **37**, 52(2019), https://doi.org/10.1016/j.jre.2018.04.013
47. F. Zaman, G. Rooh, N. Srisittipokakun, T. Ahmad, I. Khan, M. Shoaib, and J. Kaewkhao, *Solid State Sciences*, **89**, 50(2019), https://doi.org/10.1016/j.solidstatesciences.2018.12.020
48. P. Narwal, M. S. Dahiya, A. Agarwal, A. Hooda, and S. Khasa, *Journal of Luminescence*, **209**, 121(2019), https://doi.org/10.1016/j.jlumin.2019.01.042

[RJC-9618/2026]